Planck-LFI: instrument design and ground calibration strategy

M. Bersanelli[1], B. Aja[2], E. Artal[2], M. Balasini[3], G. Baldan[3], P. Battaglia[3], T. Bernardino[4], P. Bhandari[5], E. Blackhurst[6], L. Boschini[3], R. Bowman[5], C. Burigana[7], R.C. Butler[7], B. Cappellini[1], F. Cavaliere[1], F. Colombo[3], F. Cuttaia[7], R. Davis[6], X. Dupac[8], J. Edgeley[6], O. D'Arcangelo[9], L. De La Fuente[2], A. De Rosa[7], F. Ferrari[3], L. Figini[9], S. Fogliani[8], C. Franceschet[3], E. Franceschi[7], P. Jukkala[10], T. Gaier[5], A. Galtress[6], S. Garavaglia[9], P. Guzzi[3], J.M. Herreros[11], R. Hoyland[11], N. Huges[10], D. Kettle[6], V.H. Kilpelä[10], M. Laaninen[10], P.M. Lapolla[3], C.R. Lawrence[5], D. Lawson[6], F. Leonardi[12], P. Leutenegger[3], S. Levin[5], P.B. Lilje[13], P.M. Lubin[12], D. Maino[1], M. Malaspina[7], N. Mandolesi[7], G. Mari[9], M. Maris[8], E. Martinez-Gonzalez[4], A. Mediavilla[2], P. Meinhold[12], A. Mennella[1], M. Miccolis[3], G. Morgante[7], A. Nash[5], R. Nesti[14], L. Pagan[3], C. Paine[5], J.P. Pascual[2], F. Pasian[8], M. Pecora[3], S. Pezzati[1], M. Pospieszalski[15], P. Platania[9], M. Prina[5], R. Rebolo[11], N. Roddis[6], N. Sabatini[9], M. Sandri[7], M.J. Salmon[4], M. Seiffert[5], R. Silvestri[3], A. Simonetto[9], G.F. Smoot[16], C. Sozzi[9], L. Stringhetti[7], L. Terenzi[7], M. Tomasi[1], J. Tuovinen[17], L. Valenziano[7], J. Varis[17], F. Villa[7], L. Wade[5], A. Wilkinson[6], F. Winder[6], A. Zacchei[8]

Abstract – The ESA Planck satellite is designed to achieve precision imaging of the Cosmic Microwave Background with an unprecedented combination of angular resolution, sensitivity, spectral range and sky coverage. The Low Frequency Instrument is one of two complementary instruments, and covers 30, 44, and 70 GHz with an array of wide-band pseudo-correlation, cryogenic radiometers. Advanced qualification models of the radiometer chains and of the instrument electronics have been manufactured, tested and integrated into the LFI Qualification Model. The main radiometer calibration, RF tuning and performance characterization is carried out at a single radiometer chain level, and then verified at instrument integrated level in dedicated cryofacilities. Here we describe the main requirements and instrument design, and we summarize the radiometer calibration strategy optimised during the qualification activity in view of the LFI Flight Model campaign.

Index Terms – **please enter index terms.**

I. Introduction

Following the *COBE*[1] and *W M AP*[2] missions, Planck[3] is the third generation space project dedicated to observations of the Cosmic Microwave Background (CMB). Planck is designed to observe temperature anisotropies over the whole sky with a powerful combination of angular resolution (30' to 5' depending on frequency) and sensitivity ($\Delta T/T \simeq 10^{-6}$) leading to a determination of the CMB angular power spectrum limited by cosmic variance and unavoidable astrophysical foregrounds. The Planck instruments are also sensitive to polarisation and are expected to push CMB polarisation measurements beyond previously reached sensitivities. The Planck multi-frequency, high-resolution maps are expected to have profound impact on cosmology, particularly through the high-precision extraction of cosmological parameters from the angular power spectra, and will also form a rich data base for Galactic and extragalactic millimeter-wave astrophysics. The wide

Received July 15, 2005.

[1] Dipartimento di Fisica, Università degli Studi di Milano, Italy. [2] Departamento de Ingeniera de Comunicaciones, Universidad de Cantabria, Spain. [3] Alenia Spazio, Laben, Vimodrone, Milano, Italy. [4] Instituto de Fisica De Cantabria, Consejo Superior de Investigaciones Cientificas, Universidad de Cantabria, Spain. [5] Jet Propulsion Laboratory, Pasadena, USA. [6] Jodrell Bank Observatory, Jodrell Bank, U.K. [7] IASF - Sezione di Bologna, INAF, Bologna, Italy. [8] Osservatorio Astronomico di Trieste, INAF, Italy. [9] Istituto di Fisica del Plasma, CNR, Milano, Italy. [10] Ylinen Electronics Oj, Teollisuustie 9 A, 02700 Kauniainen, Finland. [11] Istituto de Astrofisica de Canarias, Tenerife, Spain. [12] Physics Department, University of California at Santa Barbara, USA. [13] Institute of Theoretical Astrophysics, University of Oslo, Norway. [14] Osservatorio Astrofisico di Arcetri, Firenze, INAF, Italy. [15] National Radio Astronomy Observatory, Charlosville, USA. [16] Lawrence Berkeley National Laboratory, University of California at Berkeley, USA. [17] MilliLab, VTT Information Technology, Esppo, Finland.

[1] http://lambda.gsfc.nasa.gov/product/cobe/

[2] http://map/gsfc.nasa.gov

[3] http://planck.esa.int

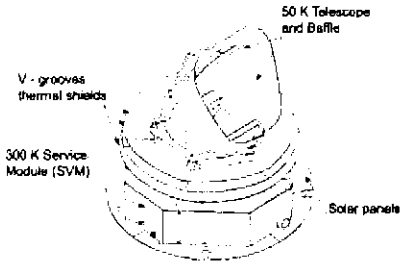

Fig. 1. Overview of the Planck satellite, showing the primary reflector, the baffle and the three thermal shields ("V-grooves") used to thermally decouple the cold (~ 50 K) telescope enclosure from the warm (~ 300 K) service module.

spectral coverage (30-850 GHz) ensures that foreground components can be precisely disentangled from the cosmological fluctuations. This is achieved by the combination of two instruments sharing the focal plane of the Planck telescope: the Low Frequency Instrument (LFI) covering the 30-70 GHz range with an array of coherent receivers cooled to 20 K, and the High Frequency Instrument (HFI), covering the 100-850 GHz range with bolometer detectors cooled to 0.1 K. The design of the Planck satellite (see Fig. 1) is largely driven by the need to thermally decouple the cold (~ 50 K) payload enclosure from the warm (~ 300 K) service module, and by radiation stray-light requirements. The Planck telescope is a shielded off-axis Gregorian system with 1.5 m projected aperture, providing the needed angular resolution and side-lobes rejection. Planck is planned to perform at least two complete sky surveys from a Lissajous orbit around the Sun-Earth L2 point, at 1.5 million km from Earth.

This paper describes the design and calibration of the Planck-LFI instrument [1, 2]. We present the main scientific and technical requirements driving the instrument design as well as the key features of the LFI pseudocorrelation receiver. Finally, we outline the calibration strategy and present sample results from the radiometer qualification campaign.

II. Requirements and design drivers

The heart of the LFI instrument is a multi-frequency array of double-profiled corrugated horns [3] feeding receivers using cryogenic indium phosphide (InP) high-electronmobility-transistor (HEMT) low-noise amplifiers. The sensitivity is substantially enhanced by operating the radiometers at 20 K. This is achieved with a closed-cycle, vibrationless, hydrogen sorption cryocooler [4] which provides 1 W of heat lift at 20 K, and also provides 18 K pre-cooling to the HFI. This

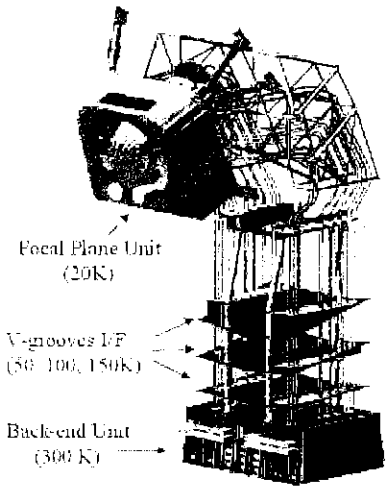

Fig. 2. View of the LFI radiometer array assembly. The frontend unit is located at the focus of the Planck telescope, and includes corrugated feed horns, the low-loss wide-band orthomode transducers, and the radiometer front-end modules (FEMs) with hybrids, cryogenic low noise amplifiers and phase switches. The composite waveguides are designed to meet simultaneously radiometric, thermal and mechanical requirements, and are thermally linked to the V-groove shields. In the back-end unit, located on top of the Planck service module at 300 K, the radiometers back-end ensured further amplification and detection, and are directly interfaced to the data acquisition electronics. After on-board processing, provided by the radiometer electronics box (REBA) located in the SVM, the compressed signal is downlinked to the ground station together with housekeeping data.

translates into stringent requirements on power consumption (~ 350 mW) for the LFI cryogenic active components, requirements that are fulfilled by splitting the radiometers into a cold front-end and a warm back-end sub-assemblies connected by a set of waveguides (see Fig. **2??**). To minimize parasitic thermal loads to the 20 K stage (~ 230 mW) a composite waveguide design is used with a straight section of gold-plated stainless steel and a twisted section in electroformed copper. The main specification of the LFI system are in Table 1.

A differential instrument concept is essential to suppress $1/f$-type noise induced by gain and noise temperature fluctuations from the amplifiers. Because the susceptibility

to most systematic effects increases with the radiometer input offset, the sky signal must be compared to a reference as close as possible to the sky temperature, i.e., the sky itself or a stable cryogenic load [5]. In the case of Planck a natural internal reference is provided by the HFI 4 K stage. In order to suppress the effects of the residual offset (< 2 K in nominal conditions) we introduce a gain modulation factor r (of order unity) in the

Table 1. LFI flight performance specification.

Center frequency [GHz]	30	44	70
Number of feeds	2	3	6
Number of detectors	8	12	24
Angular resolution [arcmin]	33	23	13
Effective bandwidth [GHz]	6	8.8	14
Noise per 0.5° pixel [mk]	8	8	8
Sensitivity [mK Hz–1/2]	0.24	0.29	0.41
1/f knee frequency [mHz]	50	50	50
Systematic error/pixel [mk]	< 3	< 3	< 3
FEM power dissipation [mW]	27	34	24

on-ground data processing, which is used to balance the radiometer output [6]. As we shall see, the QM measurements confirm the efficient suppression of instability in the measured signal difference ($T_{A,sky} - rT_{A,load}$). The $1/f$ noise arising from the warm back-end is suppressed by a fast-switching (at: 4 kHz) of the sky and load signals.

III. Receiver design

In the front-end part of the instrument the sky radiation is separated by an OMT into two perpendicular linearly polarised components that propagate independently through two parallel radiometers. In each radiometer (Fig. 3, top) the sky signal and the signal from the 4 K reference load are coupled to the cryogenic LNAs via a 180° hybrid. The reference loads provide a stable signal by means of an optimised blackbody target at ~ 4 K [7]. One of the two signals then runs through a switch that applies a phase shift which oscillates between 0 and 180 at a frequency of 4096 Hz. The signals are then recombined by a second 180 hybrid coupler, producing an output which is a sequence of signals alternating at twice the phase switch frequency. In the back-end of each radiometers (Fig. 3, bottom) the RF signals are further amplified, filtered by a bandpass filter, and then detected. After detection, the sky and reference load signals are integrated, digitised, down-sampled, and requantized before downlink.
According to this scheme, each radiometer produces two independent streams of sky-load differences. The final measurements is provided by a further averaging of these differenced data samples between the two radiometer legs.
To first order each detector power output is given by:

$$\hat{p} = ak\beta\left[\tilde{T}_{sky}(G - rI) - r\tilde{T}_{load}\left(G - \frac{1}{r}I\right) + (1 - r)T_{sky}\right], \quad (1)$$

where β is the radiometer effective bandwidth, k is theBoltzmann constant, a is the proportionality con-

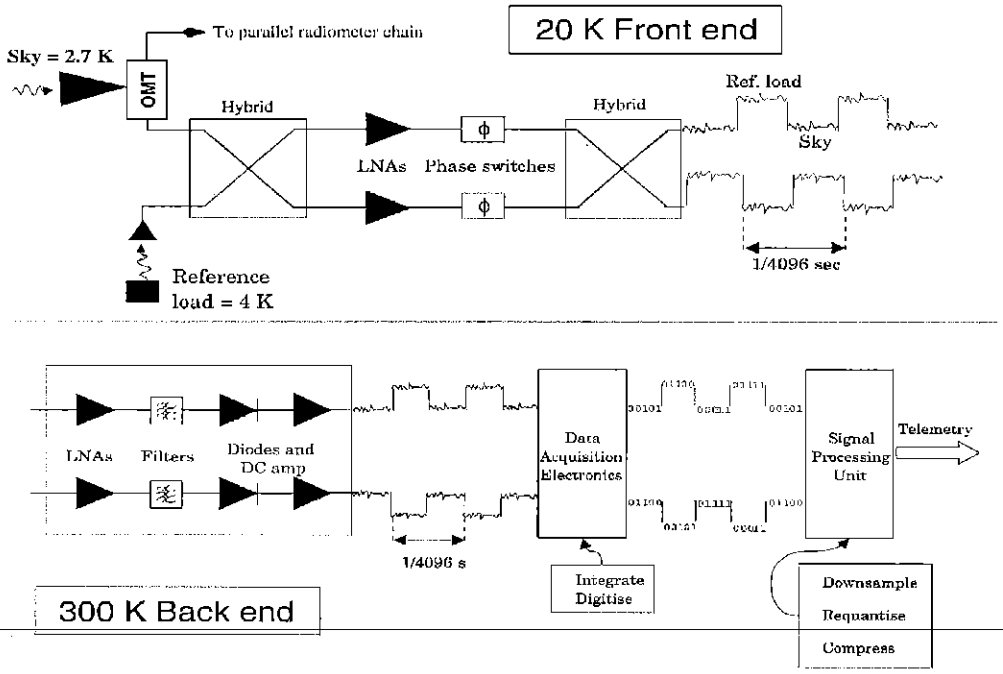

Fig. 3. Schematic of the front-end (upper figure) and back-end (lower figure) of a signal LFI radiometer. Each horn feeds two radiometers, each carrying a linearly polarised component, and each radiometer has two detectors receiving alternate sky and load signals at a rate of ~ 4 kHz.

stant of the square law detector diode, G and I are the effective gain and isolation, and r is the gain modulation factor. The terms

$$(2) \quad \tilde{T}_{\rm sky} = T_{\rm sky} L^{-1}_{\rm feed-OMT} + (1 - L^{-1}_{\rm feed-OMT}) T_{\rm phys}$$

$$(3) \quad \tilde{T}_{\rm load} = T_{\rm load} L^{-1}_{4\rm K} + (1 - L^{-1}_{4\rm K}) T_{\rm phys}$$

represent the sky and load signals at the input of the first hybrid. Here the L terms represent the insertion loss of the feed-OMT and of the 4 K reference load arms at the input of the first hybrid, while small terms from return loss and leakage are neglected for simplicity. If the isolation term is small, then the power output is nulled if

$$(4) \quad r \simeq \frac{(\tilde{T}_{\rm sky} + \tilde{T}_{\rm sys})}{(\tilde{T}_{\rm load} + \tilde{T}_{\rm sys})} .$$

In this case it can be shown [5, 6] that the radiometer is sensitive only to the $1/f$ noise caused by noise temperature fluctuations, which represent only a small fraction of the total $1/f$ noise of the front-end amplifiers, and the resulting knee frequency is linked to the load temperature by $f_k \propto (1 - r)^2$. Note also that the radiometer sensitivity does not depend (to first order) on the temperature of the reference load.

IV. Radiometers QM Campaign

The LFI demanding scientific performance (Tab. 1) and the complexity of the system required early development of radiometer models and an accurate on-ground testing and calibration plan. Early in the project, we developed prototype radiometer chains to assess the maturity of the receiver design, confirm feasibility of critical units and understand residual receiver systematics. As a second step, qualification models ("QM") of the radiometers have been produced with characteristics nearly identical to the flight models ("FM"), though not requiring full flight performances. The main purpose of the QM radiometer calibration campaign was to optimise the test and calibration procedure in view of the flight campaign, and identify criticalities in the instrument and/or measurement setup.
The basic radiometer unit is the radiometer chain assembly (RCA) comprising feed-horn, OMT, front-end module (FEM) connected to a back-end module via a set of 4 waveguides (Figs. 4 and 5). In the QM and FM, the main radiometer calibration, RF tuning and performance characterization are carried out at RCA level and then verified at instrument integrated level. Four RCAs were produced and tested as part of

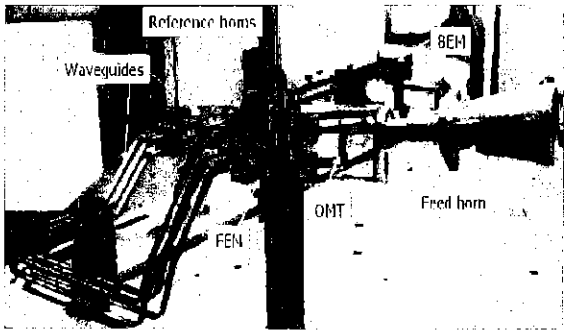

Fig. 4. 30 GHz Radiometer Chain Assembly (RCA). The four waveguides are visible, with twisted copper section connected to the FEM, and the straight stainless steel section connecting the BEM.

Fig. 5. Front-end portion of the 70 GHz RCAs in cryo facility. Two RCAs can be tested simultaneously in the 70 GHz cryofacility. On the right two feed horns are visible coupled to the sky load.

the QM campaign: one at 30 GHz, one at 44 GHz and two at 70 GHz. The RCAs were integrated from components extensively tested at single unit level (i.e., feeds, OMTs, FEM, waveguides, BEM). Optical and polarisation performances are dominated by feed horn and OMT characteristics, which have been extensively tested before integration in the QM RCAs.

A) QM optical calibration

Accurate measurements of the feed horn beam symmetry, sidelobes, and frequency dependence are needed to properly model the LFI beams through the Planck telescope, to be compared to in-flight beam measurements [8]. The phase and amplitude far field patterns of the QM feed horns were measured in the E and H planes and ±45°, at five frequencies in each band (center frequency, ±5%, and ±10%). Feed measurements

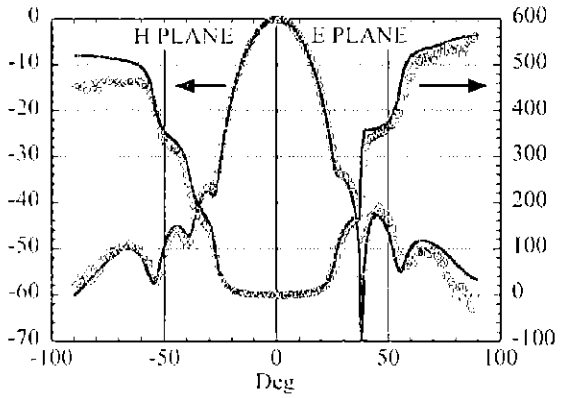

Fig. 6. Sample amplitude (left scale, dB) and phase (right scale, degrees) pattern at 70 GHz in the two principal planes. Experimental data (diamonds) and simulations (continuous line).

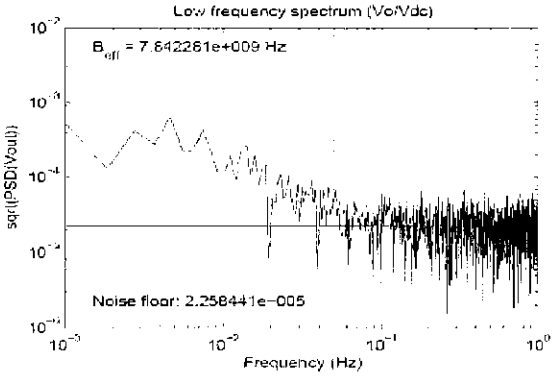

Fig. 8. Representative noise spectrum of a 70 GHz QM RCA differenced channel, after use of gain modulation factor. The stability is improved by a factor of a few thousands with respect the un-differenced signal.

were found in excellent agreement with simulations, as shown in Figure 6. OMTs specifications were rather extreme in terms of bandwidth (20%), return loss (20 dB) and isolation (–40 dB), and were designed and manufactured with strong size constraints. Insertion loss and isolation have direct impact on receiver noise temperature and polarization sensitivity, whereas input return loss at rectangular ports is needed to minimise mis-match effects at the FEM interface. The scattering parameters of OMTs were measured in a two port configuration. Figure 7 shows a sample measurement of return loss of the 30 GHz OMT terminated with the feed horn, and of the feed horn alone. The qualification model OMT isolation always exceeded –45 dB, ensuring an excellent polarisation performance. Measuring waveguides S parameters was a challenging task due to their length and complex routing. The most reliable measurement technique turned out to be the one-port-configuration, terminating the other end with a load or a short for measuring S11 or $|S12 \times S21^*|^{1/2}$.

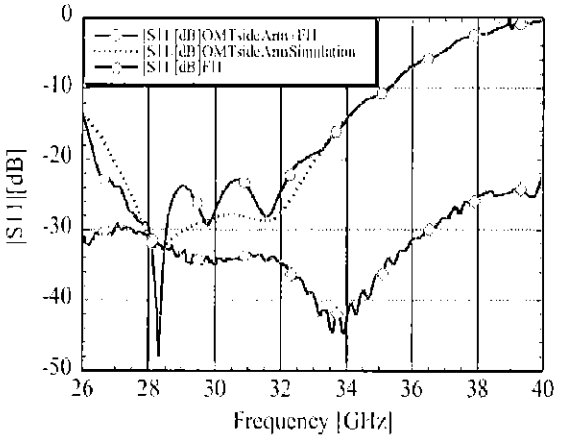

Fig. 7. Measurement of reflectivity of the feed horn (diamonds) and the OMT terminated with the feed horn (circles). The simulation of OMT side arm reflectivity is shown by the dotted curve (26-34 GHz only). The nominal radiometer bandwidth is 27-33 GHz. The distortion due to the circular to rectangular transition used for the feed horn test was removed from the data using time domain filtering (time gating).

B) Radiometer chain assemblies

A complete set of test and calibration procedures was defined and performed on each QM RCA in order to properly tune the LNA and phase switches, and to measure the main radiometer characteristics such as noise temperature, gain, bandwidth, band shape, offset, isolation and linearity. The test were performed in cryo-facilities capable of reproducing nearly the same thermal and environmental conditions as expected in

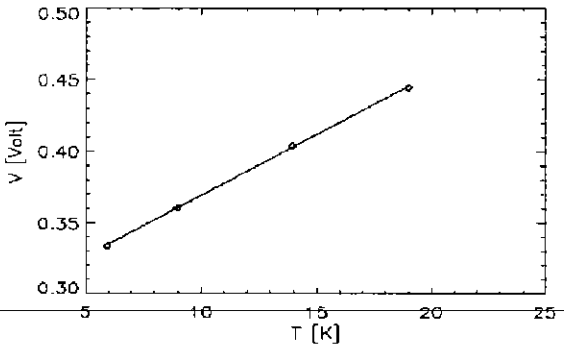

Fig. 9. Repersentative linearity test on one of the 44 GHz RCA channels. No measurable deviation from linearity (at 10^{-3} level) is observed within a temperature range as large as ΔT~18K.

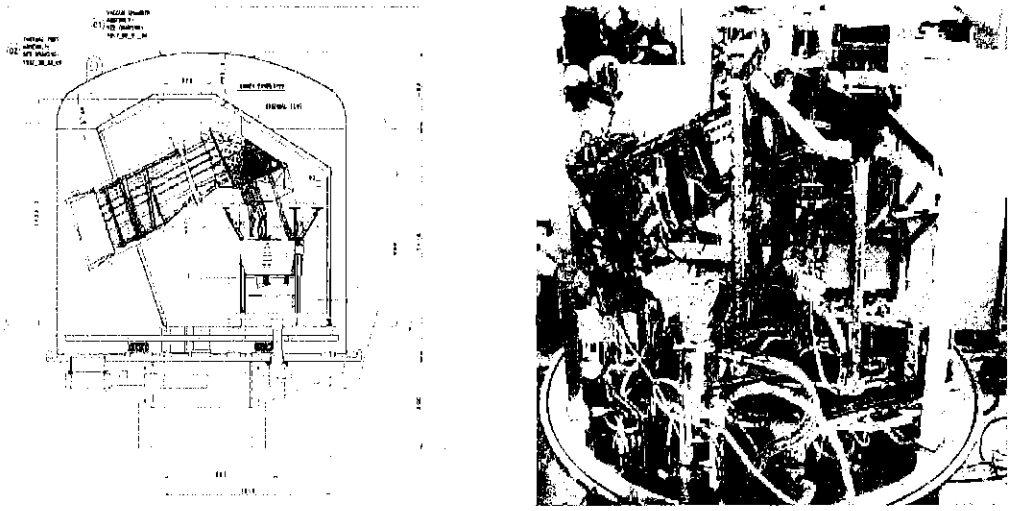

Fig. 10. Left: schematic of the large LFI cryo-chamber (~ 2 × 2 × 2 m) showing the configuration of the radiometer array assembly for instrument-level testing. Right: picture of the instrument after integration into the cryofacility with electrical and thermal connections.

flight, i.e., 20 K front-end temperature, V-grooves temperatures at waveguides interfaces (roughly 150, 100 and 50 K, respectively), and 4 K reference loads. Low return-loss "sky targets" were coupled to the feed horns, with the possibility of changing their temperature in the range 6 to 35 K. High stability (at sub-mK level) is required by the sky targets as well as reference loads to measure the residual $1/f$ spectrum of differenced data.

A typical radiometer noise spectrum (70 GHz RCA) is shown in Figure 8 for the differenced ($T_{A,sky} - rT_{A,load}$), with a knee frequency near the 50 mHz requirement (Tab. 1). Figure 9 shows a typical linearity test (44 GHz RCA), where the signal dynamic range is extended to 15-20 K, well beyond the range of the astrophysical signal to be observed during the survey. The noise and bandwidth performances of the QM models were, as expected, typically within a factor ~ 1,5 of the flight requirements. Particular care was devoted to implement a measurement of the band-shape of the RCA system at cryogenic temperature, using an input RF swept source to the feed horn through the sky load. Test results show good agreement with RF model predictions. Finally, dedicated tests were carried out to evaluate the susceptibility of the radiometers to fluctuations in thermal and electrical interfaces. The measurements yielded coefficients consistent with instrument model predictions and constraining residual systematic effects within requirements.

C) QM instrument tests

After performance calibration, the four QM radiometer chains were integrated, without disassembling, onto the LFI instrument, complete with the main-frame of the front-end unit, back-end unit with acquisition electronics, on-board electronics and signal processing (Fig. 10). Thermally and electrically representative dummies were used for the missing chains. Radiometer performances are verified at instrument integrated level in a large dedicated cryo-facility with sky and reference loads controllable in the range 20-40 K.

The QM radiometric campaign, both at RCA and instrument level, allowed the optimisation of test configuration and cryo-facility setup, and was the basis for the development of detailed test procedures as well as dedicated analysis software. These are essential inputs in view of the flight instrument calibration campaign.

References

[1] Bersanelli, M.; Mandolesi, N.: **Please enter title of the article.** Astroph. Lett. & Comm. **37** (2000), 171-180.

[2] Mandolesi, N.; Bersanelli, M.; Burigana, C., Villa, F.: **Please enter title of the article.** Astroph. Lett. & Comm. **37** (2000), 151-160.

[3] Villa, F.; **please enter all the authors' names**: **Please enter title of the article.** Experimental Astronomy **14** (2002), 1-15.

[4] Wade L.A; **please enter all the authors' names**: **Please enter title of the article**. Advances in Cryogenic Eng. **45** (2003), 499-506.

[5] Seiffert, M.; Mennella, A.; Burigana, C.; Mandolesi, N.; Bersanelli, M.; Meinhold, P.; Lubin, P.: **Please enter title of the article**. Astronomy & Astrophys. **391** (2002), 1185-1197.

[6] Mennella, A.; Bersanelli, M.; Seiffert, M.; Kettle, D.; Roddis, N.; Wilkinson, A.: **Please enter title of the article**. Astronomy & Astrophys. **410** (2003), 1089-1100.

[7] Cuttaia, F.; **please enter all the authors' names: Please enter title of the article**. Nuclear Instr. & Methods in Phys. Res. A **520** (2004), 1-3, 396-401.

[8] Burigana, C.; Natoli, P.; Vittorio, N.; Mandolesi, N.; Bersanelli, M.: **Please enter title of the article**. Experimental Astronomy **12** (2001), 87-106.

Marco Bersanelli is Professor of Astrophysics at the University of Milano. He works in the field of observational cosmology, particularly observations Cosmic Microwave Background (CMB). He graduated in Physics at Milano University in 1986 and worked at the Lawrence Berkeley Laboratory, University of California, until 1991. He designed and built microwave radiometers for CMB spectrum experiments in the 1-90 GHz range and participated in observational campaigns at the White Mountain Research Station, University of California, and Amundsen-Scott South Pole Station, Antarctica (1986-1992). He then worked as Senior Researcher at Istituto di Fisica Cosmica, CNR, Milano, until 2000. Since 1992 prof. Bersanelli has been deeply involved in the design and development of the ESA Planck mission, designed to produce precision full-sky maps of the CMB temperature and polarisation. He is the Instrument Scientist of Planck-LFI, a radiometer array based on cryogenic HEMT low noise transistor amplifiers. He has been a member of the Planck Science Team since its first onset in 1993. Prof. Bersanelli has also contributed to sub-orbital microwave experiments, such as "BEAST" and "GEM", studies of galactic diffuse radio emissions, multi-frequency observations of AGNs, atmospheric emission in the IR and microwaves. Prof. Bersanelli is a member of the Scientific Committee of INAF (Istituto Nazionale di Astrofisica) and vice-president of CIFS (Cosnsorzio Inter-Universitario di Fisica Spaziale).